Júlio César Beja Costa

Licenciado em Micro e Nanotecnologias

Fabrication and Characterization of Transparent Conductive Oxide Surface Sensors for Electrocorticography – TrECoG

Dissertação para a obtenção do Grau de Mestre em Engenharia de Microelectrónica e Nanotecnologias

Orientador: Adam Kampff, Professor Doutor,

Champalimaud Centre for the Unknown

Co-Orientador: Elvira Fortunato, Professora Doutora,

Faculdade de Ciências e Tecnologias da Universidade Nova de Lisboa

September, 2015

Fabrication and Characterization of Transparent Conductive Oxide Surface Sensors for Electrocorticography – TrECoG

Faculdade de Ciências e Tecnologias

Universidade Nova de Lisboa

Acknowledgements

This master's project proved to be one of the most enjoyable headaches I've ever had. As everything in life, it had its ups and downs, promises and disappointments, but every step of the way was easier because I had the chance of being surrounded by the most intelligent and funny people I've ever met.

To Dr. Adam Kampff, thank you very much for receiving me in your group. At the beginning, the idea of jumping from nanotechnology to neuroscience seemed impossible, and honestly, I still believe it is close to impossible to understand neuroscience, even for neuroscientists! Nevertheless, everything felt easier because I always knew that any questions or thoughts could be discussed with my coordinator in a relaxed but detailed way, making the transition which once seemed impossible, a pleasant conversation where I had the chance of learning a small piece of the endless wonders of neuroscience.

I would like to thank Dr. Elvira for the knowledge acquired during these 5 years at the University and for the role that the Professor maintains as a beacon of the Portuguese and International scientific investigation, which contributed to the creation of the fantastic degree that I am now completing.

To Joana Neto, for all of your patience, for the long hours in surgery and the days spent looking at the computer screen. But most of all, I would like to thank Joana for the amazing ability of teaching me without ever losing her good mood, never did I see her frown, not when we were starving during surgery, or even when I repeated the same mistakes during the data analysis. Thank you!

To Dr. Joana Vaz Pinto, my guardian angel at the University. I do not believe what I've done could be possible without her help. As her "adopted" student and without her having any obligation whatsoever, Joana Vaz Pinto helped every step of the way, sometimes even with more enthusiasm than myself, regardless of gaining nothing from it but the constant headache of dealing with me.

To all of the Intelligent Systems Lab at CCU, thank you for the laughs and the stories, but most of all, thank you for the opportunity of learning with you.

To all who belong to CENIMAT and CEMOP, for having the time to help me during my project, no one had any obligation, but there is always someone available to help, and I think that is amazing.

"There is no better time than the University", I often heard, and it is true. But it isn't just the careless freedom that makes it amazing, because I would rather live in a prison with the friends I've met during these 5 years, than in a castle alone. Of all, the ones who took a special place in my life, my family "abroad", were the ones who belonged to Basolho. To Pedro Figueiredo and Moisés Tereso, for their help

since the first day I've stepped in the University. To Diogo Vaz for the afternoons spent listening to music and talking about everything and nothing, to Nuno Coelho for always being present through thick and thin, to Tiago Rosado for his companionship and by showing me the best beach in Portugal and to Jacinto for all the conversations and his ability giving the best advices. There are many others whom I will never forget, João Rosa, Afonso, Carreiras, Sofia, Joana and Constança. We were once a great family, and we shall continue a great family, just geographically apart!

To my friends back home, Tiago, Francisco, Carla and Paulo. We once dreamed of being a rock band, of having matching tattoos, for which I'm still waiting. Some of you have been there since I was 3, others not for so long, but the important thing is that no matter how far, we will always have time to sit in a coffee shop during some weekend, and for a moment, we will be in high school once again.

To my family, my Dad, Júlio, Mom, Ana, and little Brother, João. My Dad always has the best advice, but I'm his son, so I'm wired this way, nevertheless, I believe this with all my heart, we are a team, and I will always come back home. To my Mom, always worried, always giving advices, and, although hard to admit, always right. Thank you Mom and Dad, for the sacrifices you underwent in order for me to be here today. To my Brother, thank you for being amazing. As an older brother I often think of you and feel proud, you're confident, intelligent and respectful, a great man, and I'm happy to be able to stay by your side in the adventures which are yet to come.

Finally, to my girlfriend, the most important half of our Dream Team as far as I'm concerned, Marta Machado. I doubt that I could have ever asked you anything more than what you've given to me. The smiles, laughs, adventures and expectations. But most of all, thank you for the peace of mind which you've provided, thank you for always being there for me.

Resumo

Compreender o funcionamento cerebral sempre foi um dos grandes objetivos da humanidade. Este desejo incentiva a comunidade científica para a procura de novas técnicas capazes de adquirir a informação complexa que é produzida no cérebro de forma constante. A Electrocorticografia (ECoG) é uma dessas técnicas. Ao se colocarem elétrodos condutores na superfície da dura, ou até diretamente em contato com o córtex, torna-se possível medir variações de tensão elétrica que espelham a ativação da zona cerebral que é coberta pelo elétrodo. Neste trabalho, é proposto o desenvolvimento de ECoGs transparentes (TrECoG) através da deposição de filmes finos dos óxidos condutores *Gallium-Zinc-Oxide* (GZO) e *Indium-Zinc-Oxide* (IZO). Cinco dispositivos distintos foram fabricados através da técnica de deposição física *sputtering,* tendo os padrões sido definidos por *shadow-masking* e fotolitografia. Os dados adquiridos e apresentados neste trabalho validam os TrECoGs fabricados como dispositivos eficientes para adquirir informação da atividade cerebral. Os melhores resultados foram obtidos para o TrECoG com elétrodos de GZO com 500 µm de diâmetro, o qual apresentou uma impedância média de 36 kΩ para as medidas a 1 kHz. A transparência destes dispositivos atingiu valores próximos de 90% para o espetro visível. Os dispositivos que recorrem a IZO como o material condutor apresentaram valores mais elevados de transparência, porém, as impedâncias oscilaram entre 40 kΩ e 100 kΩ para as mesmas condições que os dispositivos de GZO.

Abstract

Understanding how the brain works has been one of the greatest goals of mankind. This desire fuels the scientific community to pursue novel techniques able to acquire the complex information produced by the brain at any given moment. The Electrocorticography (ECoG) is one of those techniques. By placing conductive electrodes over the dura, or directly over the cortex, and measuring the electric potential variation, one can acquire information regarding the activation of those areas. In this work, transparent ECoGs, (TrECoGs) are fabricated through thin film deposition of the Transparent Conductive Oxides (TCOs) Indium-Zinc-Oxide (IZO) and Gallium-Zinc-Oxide (GZO). Five distinct devices have been fabricated via shadow masking and photolithography. The data acquired and presented in this work validates the TrECoGs fabricated as efficient devices for recording brain activity. The best results were obtained for the GZO- based TrECoG, which presented an average impedance of 36 kΩ at 1 kHz for 500 μm diameter electrodes, a transmittance close to 90% for the visible spectrum and a clear capability to detect brain signal variations. The IZO based devices also presented high transmittance levels (90%), but with higher impedances, which ranged from 40 kΩ to 100 kΩ.

Abbreviations

AP Action Potential

BMI Brain-Machine Interface

EEG Electroencephalography

ECoG Electrocorticography

fMRI Magnetic Resonance Imaging

MUA Multi-Unit-Activity

G/R Ground and Reference electrodes

GZO Gallium Zinc Oxide

ITO Indium Tin Oxide

IZO Indium Zinc Oxide

LFPs Local Field Potentials

OECTSs Organic electrochemical transistors

Pl Photolithography

PBS Phosphate buffered saline

SNR Signal-to-noise ratio

SM Shadow Masking

SMPs Shape memory polymers

TrECoGs Transparent Electrocorticography sensors

ZIF Zero insertion force

Contents

List of Figures

1. Introduction

The mission to understand how the brain works is daunting, since there isn't a perfect technology capable of simultaneously monitoring all 85 billion neurons [1]. Nevertheless, two techniques emerge, measuring the activity from single units through the insertion of microelectrodes in the brain, or measuring the neural summed activity of large brain areas – Electroencephalography (EEG), Electrocorticography (ECoG), or functional Magnetic Resonance Imaging (fMRI). Inserting microelectrodes in the brain allows the acquisition of data from small groups of neurons, or even isolated neurons, and is the technique that presents the highest spatial resolution [2]. Recent microprobes present on-site amplification [3] - thus increasing their signal-to-noise ratio (SNR) - and biocompatible coatings that decrease their impedance level and/or increase their biocompatibility [4] [5], but still represent the most invasive technique and, due to this fact, scaling up the microelectrodes to cover the entire cortex is hard. Electroencephalography is the least invasive of all techniques [6] but it is also the technique with the lowest spatial resolution, although still sufficient for some Brain-Machine Interface (BMI) applications that only require information on whether large parts of the brain are active or not [7]. ECoG emerges as a technique that is less invasive than the microelectrodes and has an increased spatial resolution compared to that of the EEG. ECoGs detect the summed electrical activity of the neurons located in their vicinity. In order to understand this signal one must first comprehend how the basic blocks (neurons) of the brain work.

1.1. Action Potential

The standard neuron (figure 1.A) has four different morphological regions, each with its own function and characteristics: The cell body (*soma*) (1), the axon (2), the dendrites (3) and the presynaptic terminals (4). [8] The cell body contains the genetic data, and can also act as a receiver of signals from other neurons, it is also from this structure that the axon and the dendrites emerge. Dendrites are small structures which act like branches that receive information from nearby cells. The axon is a long, thin structure that emerges from the *soma* and its main responsibility is to lead information to the presynaptic terminals - where the information will pass to the post synaptic dendrites of the next neuron. Through these structures, each neuron is able to receive stimulus from other neurons (the cell body and the dendrites), distinguish and define where to convey the information received (cell body), generate an Action Potential (AP), and propagate it through the axon (axon – presynaptic terminals). The AP is a fast variation (1 kHz) of potential nearby the soma and could be detected with microprobes. At rest, the extracellular surface of the soma and axon are positively charged, whereas the cytoplasmic surface is negatively charged – the intracellular/extracellular potential at this stage is approximate to -60 mV as shown in figure 1. When a

stimulus is applied to the neuron, special gates in the membrane open at the beginning of the axon, destabilizing the previous equilibrium by increasing the permeability of the membrane to Na^+. This increase of the positive ion in the intracellular medium generates a positive potential, which destabilizes the next gate, and through this mechanism, propagates as a signal of approximately 100 mV along the axon. This ion flux is responsible for a phenomenon called volume conduction, which is explained by the movement of ions in the brain matter originated from this activity. This volume conduction generates an overall potential, which represents the summed activity of large populations of neurons and can be detected through techniques like ECoG. These bulk activities are called Local Field Potentials (LFPs) or Multi Unit Activity (MUA), depending on their frequency.

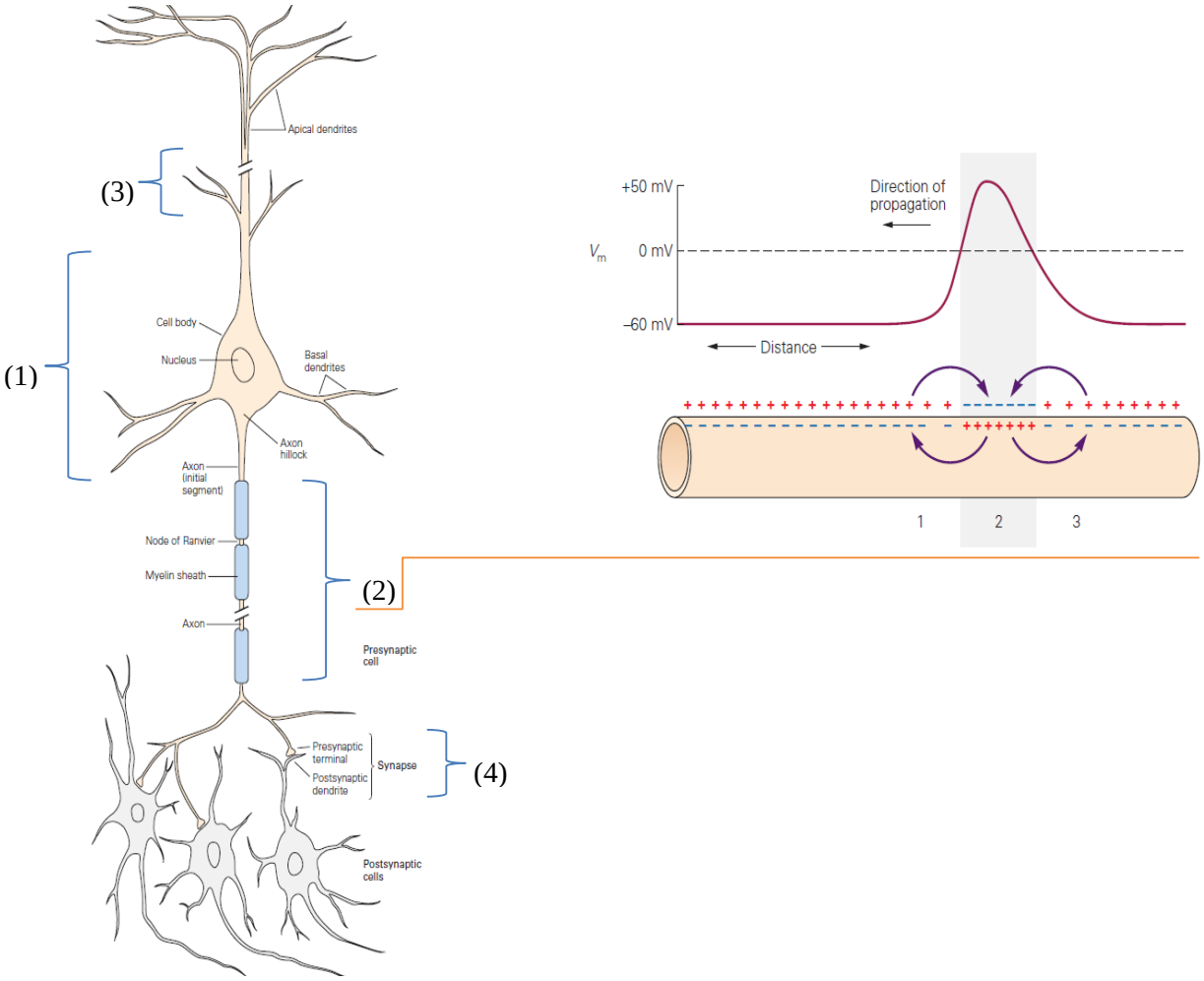

Figure 1 – Descriptive image of a neuron, the basic block of the brain, responsible for transmitting, processing and storing data in the brain. Adapted from [8],

1.2. LFPs and MUA

LFPs and MUA represent the combined electrical activity within a volume of neural tissue [9] and are obtained by filtering the raw data from the brain in different frequencies bands. LFPs represent the low-passed signal (<300 Hz) and might be generated by membrane currents of the neurons in the local neighborhood of the recording electrode. [10] This signal is divided in five different frequency zones: delta (1 Hz - 3 Hz), theta (4 Hz – 8 Hz), alpha (9 Hz - 15 Hz), beta (16 Hz - 25 Hz) and gamma (25 Hz – 300 Hz). On the other hand, MUA, a signal that is linked to the APs from local neurons, is obtained by filtering the raw data from the brain for signal over 300 Hz. LFPs have already been correlated with many perceptual and cognitive functions. An increase in the gamma activity has been linked to increased activity of the visual cortex of monkeys after being exposed to a controlled visual stimulation [11] and recent studies indicate that brain signal oscillations might also be linked to encoding perceptual experiences into memory representations by coordinating spatially distributed and co-activated neuronal groups [12]. In figure 2, a scheme of the human brain and different types of techniques and signals are shown. The insertion of microelectrodes into the brain allows the detection of APs, LFPs and MUA, but it is highly invasive. On the other hand, the signal shown for the ECoG represents MUA and LFPs and in this case no APs can be detected. Brain activity hypothesis allow the development of models for the integration of the data obtained through ECoG, thus enabling the utilization of these systems to reveal more complex brain functionalities. For example, predictive coding is nowadays the dominant paradigm in cognitive neuroscience. This theory supposes that the brain is a statistical organ constantly generating hypothesis about the state of the world, which are then tuned through the data obtained from sensorial inputs. This communication is thought to be organized in a top-down formation where predictions occur in higher hierarchical levels, and prediction errors – the difference between prediction and sensory inputs – occur at lower hierarchical levels and are then returned to the higher predictive hierarchical levels. This type of forwards/backwards communication leaves a fingerprint which can be detected in LFP signals, thus revealing this signal's potential to reveal crucial information regarding brain activity [14].

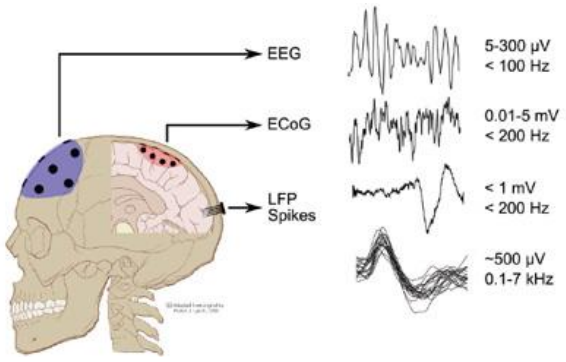

Figure 2 – Different brain signal relies on the recording tool. Adapted from [13]

One of the main reasons to record LFP/MUA signals with ECoG electrodes is the fact that being possible to record multiple brain areas simultaneously makes possible to understand the communication between them and since is a 'less' invasive technique, it isn't rejected by the body as fast as the microprobes.

Recent studies indicate that, independently of their frequency, LFPs spread over more than 1 cm away from their origin [15], challenging the idea that LFP recordings typically integrate over extremely circumscribed local domains. These signals now appear to be a mixture of "volume conducted" potentials from distant sites.

1.3. TrECoG

Designing electrodes for neural interfacing applications requires important considerations regarding materials. The most important factors to be considered are: device stiffness, biocompatibility, dielectric properties and conductivity properties. Regarding device stiffness, this characteristic is one of the most important, being deeply related with the stability of the device and its ability to conform to the non-uniform, curvilinear neural surfaces, such as the cerebral cortex. For this purpose, polyimide and Parylene (~5 GPa modulus) represent the most common choices for device substrate, nevertheless, these are not the only choices and recent studies have tried to employ shape memory polymers (SMPs) which are thermal and water sensitive, such as the Poly(MA-co-IBoA-co-AA). This type of material softens when in contact with live brain tissue, decreasing its modulus to 100 kPa – closer to the 1-10 kPa reported for the brain [16]. Other approaches use open architectures and dissolvable device substrates, which have higher modulus but also have higher biocompatibility. Comparisons between a Parylene C "mesh" type ECoG with traces in order to ease tissue regenerations and a standard Parylene C ECoG showed that the first type allows for tissue regeneration above and around the device, whereas the second favors tissue regeneration between the electrodes and the brain surface, which increases the noise and decreases device stability [17]. Silk has also proven to be an efficient support in order to ease device implantation, experiments used this natural polymer as a substrate for a 2.5 μm thick polyimide insulated device, the silk acted as a stiff support and dissolved away within 1 h after implantation, enhancing the quality of the recording signals [18]. Regarding electrode material and configuration, some innovative possibilities have been proposed, such as using organic electrochemical transistors (OECTs) with a PEDOT:PSS semiconductor channel and the gate being in direct contact with the brain surface [19], nevertheless, this approach resulted in low stability devices when compared to the more common Au, Pt, PEDOT devices. Au or Pt electrodes are the most common devices, whether for EEG [20] or ECoG [21] [22]. Impedance values for the brain/electrode interface for 1 kHz are considered a 'benchmark' measure. By lowering the impedance of the contacts, the SNR increases and brain signal can be acquired with increased resolution. Acceptable impedance values are found to be between 1 kΩ and 100 kΩ [21] [22] [23]. The NeuroGrid [24] is probably the ideal state-of-the-art regarding ECoG devices. This device has 10x10 μm^2 PEDOT:PSS electrodes, which matches the average size of neuronal bodies and neuronal density. This system is reportedly capable of isolating single-neuron action potentials and is the most advanced system of its kind.

These sensors have been widely used for clinical and investigation purposes, nevertheless, creating transparent electrodes offers new possibilities for the optical monitoring or manipulation of neural activity and concurrent data acquisition, thus increasing the versatility of these devices by allowing them to be used alongside with techniques such as Optogenetics.

In this work, the development of two Transparent Electrocorticography sensors is proposed, the GZO and IZO TrECoGs. Previous works produced Indium Tin Oxide (ITO) ECoGs [25] and Graphene Sheet ECoGs [26] (figure 3), which have be validated as efficient devices. In this work, GZO and IZO are tested in order to validate new TCO materials.

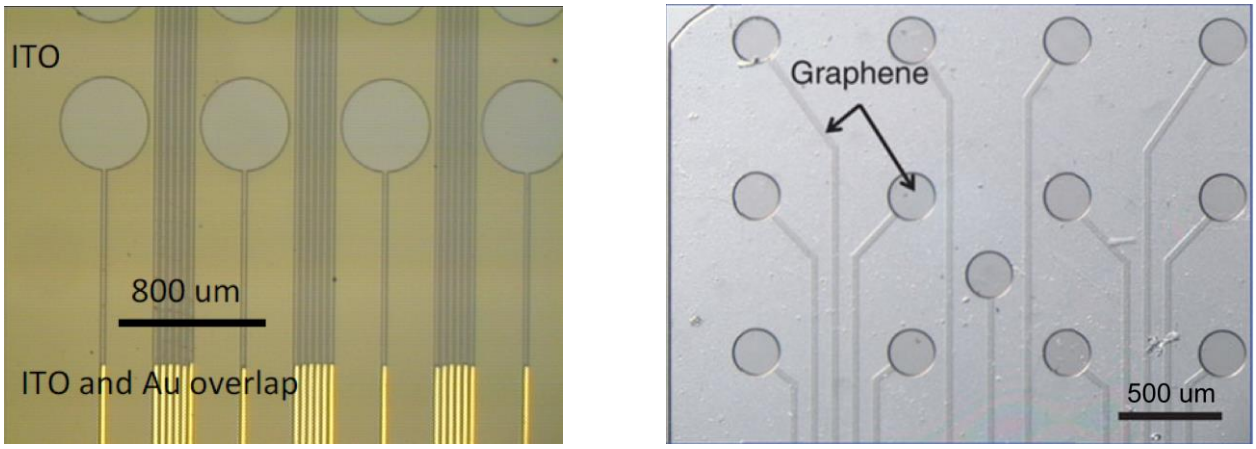

Figure 3 – Transparent electrodes previously fabricated with ITO (left) and graphene sheets (right). Adapted from [23 and 24]

TCOs are a promising class of materials which display a remarkable combination of high electrical conductivity and optical transparency [27]. This type of material is widely spread in various important technological applications, such as the flat displays and solar energy harvesting panels. The transparency and conductivity of TCOs can be explained by the doping of semiconductor materials with shallow donors. Semiconductors show band gaps in the range of 3 – 4 eV, making them transparent to visible wavelengths, subsequently, in the absence of donor or accepter states, thermal excitation across the band is negligible, no free carriers are present and the Fermi level is positioned mid-gap, making these materials insulators, as shown in figure 4. Nevertheless, if a population of shallow donors is present – for example, when Sn^{4+} substitutes In^{3+} in In_2O_3, Sn^{4+} forms ionic bonds with the surrounding oxygen, and contributes with a single shallow donor – the Fermi level rises and approaches the conduction band, at this point thermal excitation is sufficient to promote electrons from the donor state into the conduction band as described by a Boltzmann distribution. At low concentrations, the Fermi level remains within the band gap. However, if the density of these states increases as more states are added, at a critical density, known as Mott transition point, the impurity band and the conduction band merge, so that the Fermi level is effectively pushed into the conduction band. When this level is reached, the materials have a permanent (degenerate) population of

free charges, nevertheless, its direct band gap remains in the range of 3 – 4 eV, making it transparent while simultaneously conductive.

GZO [29] and IZO [30] are doped semiconductors. For GZO, Zn^{2+} is substituted by Gallium, whereas for IZO it's In which is substituted by the Zn ions until the Mott transition point is reached. It is important to note that the ion O^{2-} is present in metal oxide systems as the initial shallow donor, as these originate from the native defects from the oxygen vacancy. It is also important to understand that oxygen vacancies typically occur naturally as deposited material.

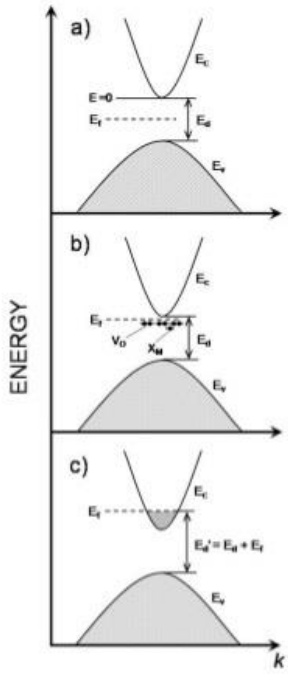

Figure 4 – Band-gap schematics for three different doping concentrations. Adapted from [28]

2. Fabrication and Characterization

The work conducted during this master's thesis consisted on the fabrication of IZO and GZO transparent surface electrodes (TrECoGs) for detection of Local Field Potentials (LFPs) and Multi-unit activity (MUA) above the cortex.

In this chapter, the fabrication process is explained for all devices, as well as the characterization techniques. In order to validate the fabricated devices' electrical performance, *in vivo* recordings were conducted on anesthetized rodents. To validate the use of these devices in parallel with optogenetic techniques, an incident green collimated light (532 nm) was used on the electrodes. That protocol allowed the establishment of possible electric artifacts due to the laser beam.

2.1. Device Fabrication

Five types of devices were fabricated on Parylene C substrates. Shadow masks (SM) and photolithography masks (PL) were designed and produced to pattern the electrodes. Two different TCOs (IZO and GZO) were evaluated, and to improve the adhesion of the layers to parylene, plasma treatments were also performed: PL0 means no treatment applied, Pl1 indicates O_2 plasma etching to improve TCO adhesion to the Parylene C substrate, and Pl2 indicates an extra plasma treatment equal to the one performed for the Pl1 devices but for the TCO/Metal interface – this treatment is applied after TCO deposition. A final parylene encapsulation step was performed. In figure 5, a simplified diagram presents the process chain; all key points will be further explained (figure 5).

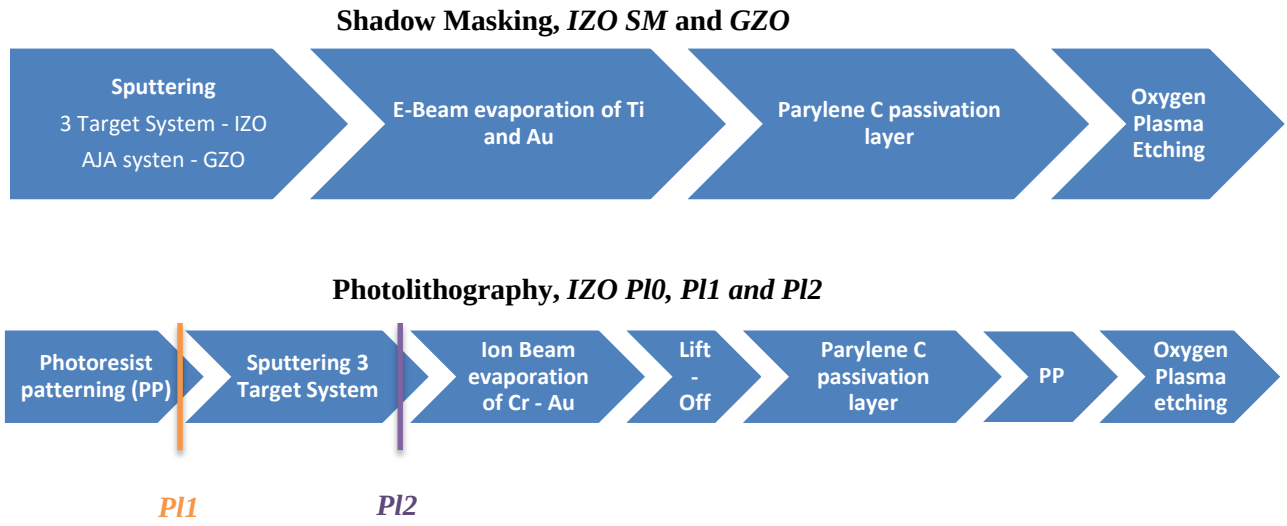

Figure 5 – Schematic of the fabrication procedures of all the fabricated devices in this work.

2.1.1. Photolithography – IZO Pl0, Pl1 and Pl2

Positive photoresist 1518 was deposited and spread through spinning on the surface of a 10 µm Parylene C thin film previously deposited on a 10x10 cm glass substrate. The photoresist then underwent a soft bake process for 1 min and 20 s at 120 ˚C – Parylene C is expected to survive continuous exposure to air at 80 °C for 10 years and regular non-continuous exposures up to 220 °C. Photoresist patterning was attained through UV exposition on a Karl Suss MA 45 Mask Aligner, according to the pattern defined by the design shown in Appendix A. The process was finalized by etching the exposed photoresist with an AZ 726 MIF developer. This process was once again repeated for the definition of the areas to be etched for contact opening (3.1.6).

2.1.2. TCO deposition

3" IZO and GZO targets (± 200 nm) were sputtered and deposited on Parylene C substrates. IZO SM and GZO SM patterning was achieved through shadow masking during deposition. This process requires personalized masks (Appendix A), fabricated from a 1 mm thick aluminum sheet, where the pattern is cut by a Gravograph IS400 with the blade positioned at a 10˚ angle to the surface perpendicular – this minimizes the deposition shadow effect, which could otherwise decrease line width (500 µm). IZO depositions took place in a 3 Target Sputtering Deposition System, whereas GZO depositions took place in an AJA ATC 1300 system. Deposition conditions are present in Appendix B for both the IZO and GZO depositions. Fig 6.

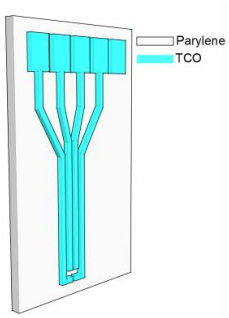

Figure 6 – Patterning of the TCO layer.

2.1.3. E-Beam Evaporation

Au (± 60 nm), Ti (± 6 nm) and Cr (± 6 nm) crucibles were evaporated with an in house E-Beam equipment, thus metalizing the TrECoG lines (excluding the electrode area) and ZIF contacts. Gold was used as a material to reduce line resistance and to improve the contacts between the devices and the zero insertion force (ZIF) connectors. Chromium and Titanium were used to improve TCO-Au adhesion.

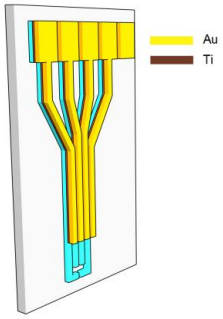

Figure 7 – Metalization schematic.

2.1.4. Lift Off - IZO Pl0, Pl1 and Pl2

For the lift off of the photoresist, the samples were placed in acetone during 2h, followed by 20 minutes of brushing in order to minimize structural damage.

2.1.5. Parylene Substrate and Passivation Layer Deposition

The substrates used for the IZO Pl0, Pl1 and Pl2 TrECoGs were deposited through the sublimation of 10 g of Parylene C by a *SCS specialty coating systems PDS 2010*, whereas the substrates used for the IZO SM and GZO SM were recycled residues from the system walls. For the final passivation layer, only 3 g were used, for a theoretical thickness of 1.5 µm.

2.1.6. Plasma Etching

A 20 sec Soft Plasma treatment was applied in order to create slight morphological depressions in the Parylene C substrates (PL1), as well as to activate bonds between the TCO and the Cr layer (Pl1 and Pl2). This process took place on a plasma etching system (RIE Trion). Plasma etching was also used as a final technique to etch the parylene passivation layer, simultaneously opening windows for the electrode/brain and contact/ZIF interfaces. Conditions for these processes vary according to the material on the surface of the sample and its thickness, for these devices such conditions are present in Appendix B.

2.2. Electrical, Optical and Morphological Characterization

2.2.1. Electrochemical Impedance (EI)

Electrodes were immersed in phosphate buffered saline solution (PBS) and a NanoZ (Neuralynx) was used to characterize impedance at 1 kHz, with a two electrode cell configuration –TrECoGs were connected to a ZIF, each channel acted as working electrodes and the reference electrode was an Ag/AgCl wire (Science Products GmbH, E-255).

2.2.2. Spectrophotometry

Transmittance measurements were taken with a PerkinElmer Lambda 950 UV/VIS/NIR Spectrometer. For the IZO SM samples, measurements were taken for the 250 nm – 800 nm portion of the light spectrum, whereas for the GZO SM and IZO Pls the interval was 200 nm – 1500 nm

2.2.3. Profilometry

For these measurements, an Ambios XP-200 was used**.** The samples used to evaluate film thickness originated from glass substrates which underwent the TCO deposition for the GZO SM and IZO SM devices, as well as the metal and Parylene passivation layers.

2.3. In Vivo recordings

2.3.1. Whisker stimulation and Barrel Cortex measurements

For these recordings the GZO SM device was tested. These tests were conducted on a Long Evans rodent, whose head was stabilized in a stereotaxic frame. The test subject received intraperitoneal injections to maintain a controlled state of anesthesia (1 g/10 mL for Ketamine and 1 mg/1 mL Medetomidine). A 4 mm (diameter) craniotomy was performed on the left hemisphere of the rodent's skull, exposing the barrel cortex area, contra-laterally to the stimulated whiskers. The TrECoGs were connected to a ZIF with 36 contacts (device sheet in Appendix C). The signal was then amplified, filtered and multiplexed for the 32 channels through a RHD132 (InTanTech, USA) (device sheet in Appendix E) electrophysiology interface chip, which conveyed the information to an open-source electrophysiology acquisition board (Open Ephys).

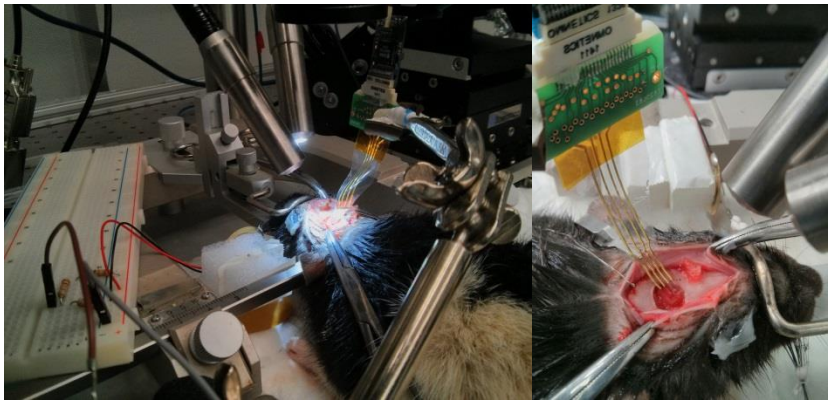

Figure 8 – Apparatus required for *in vivo* recordings of LFPs.

In addition to the recording system apparatus, a piezoelectric microphone and a voltage divider were added, (figure 8) with the output connected to the analog input of the Open Ephys. This apparatus allows a time coherent correlation between the whiskers movement and the signal recorded through electrodes. Control measurements were made by the ipsi-lateral whiskers activation. All data was recorded with the Bonsai software [31] during10 min with a 30k samples/s rate. The raw data was then processed in Python (NumPy:Spyder) (for informations regarding the code used, please refer to Appendix D): the microphone signal peaks, i.e. hits, were found by considering a 0.1 V threshold, and a minimum 2500 samples refractory interval in order for the program to exclude the reminiscent piezoelectric vibrations after each hit. The raw brain data was normalized, filtered by a notch in order to remove the 50 Hz noise, low passed at 150. Finally, the activity that corresponded to the same samples as those of the piezoelectric activity were aligned and shown in an interval of ±100 ms. Data analysis is presented in the next chapter.

2.3.2. Laser light pulse

Response to optical stimulation was performed for the IZO Pl0 and GZO SM devices in order to compare differences caused by different electrode materials.

These tests were conducted on a frame containing agar, a solution that simulates the surface of the brain. The light emitting device used for this experiment was a laser from Laserglow Technologies, model LCS-0532-TSD-00150-05, with an average output of 177.4 mW, mounted on a Thor Labs support (figure 9). All data was recorded with the Bonsai software, with a 30k samples/s rate. An Arduino board, generating square waves with 500 ms, 2 s and 10 ms periods, controlled the laser. This signal was then processed in a voltage divider which decreased its amplitude by an order of 10 and finally conveyed to the analogical input of the Open Ephys.

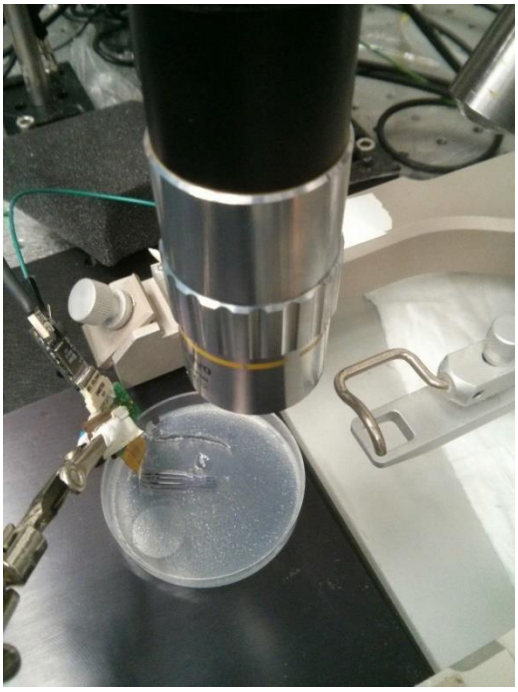

Figure 9 – Apparatus required for laser noise generation assessment.

3. Results & Discussion

In this chapter, characterization results of the optical, electrical and morphological characteristics of the devices fabricated are presented. In figure 10.a, an example of an IZO SM device is shown, all other devices are equal, and thus are not presented. These devices have a 4 electrode configuration, following the orientation in figure 10.b. These devices have 500 µm electrodes with a 250 µm electrode pitch.

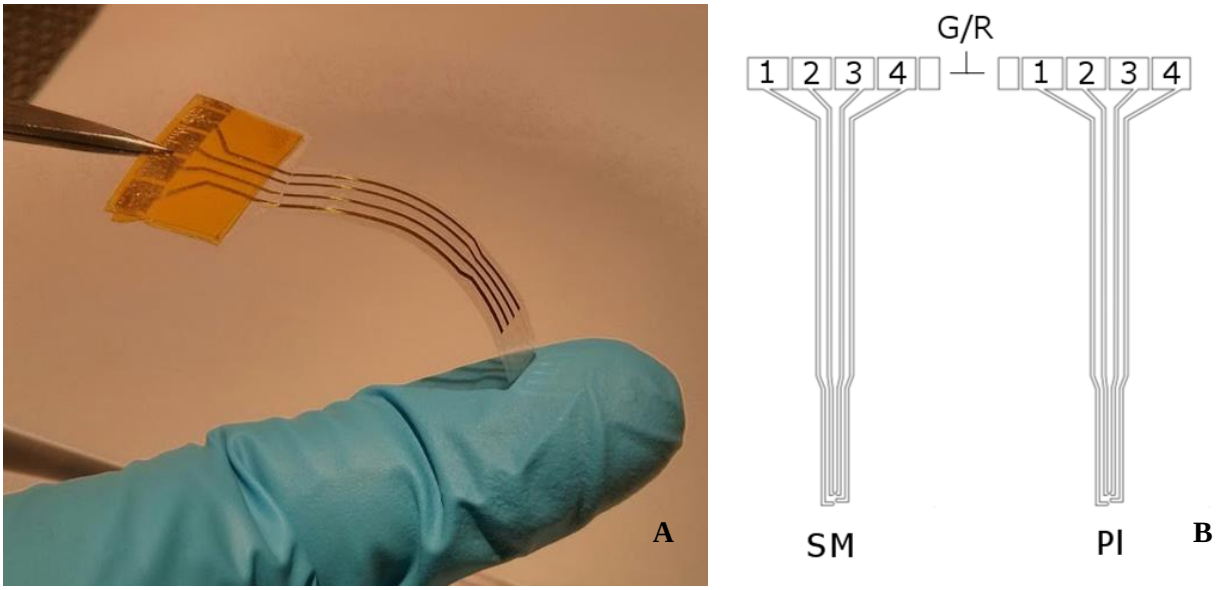

Figure 10 – IZO SM device fabricated (A) and design of the electrodes fabricated (B). The yellow material seen in image A represents the Kapton used in order to adjust the device thickness for the insertion in the ZIF mechanism.

The first devices were patterned through Shadow-Masking (SM) and the electrode number 1 of this design (Fig10 b) was short-circuited with the G/R due to the ZIF G/R position, which is on the right, thus coinciding with the 1st electrode of the SM devices. For this reason, the 1st electrode of the SM TrECoGs is not considered in all experiments. The design for the Photolithography (Pl) patterned TrECoGs generated 4 functional electrodes, thus solving the problem previously explained. Each electrode is addressed by 8 channels in the ZIF connector, this device has a 36 channel configuration, 32 for signal acquisition and 4 on the right for the G/R. For more information regarding this subject, please refer to the datasheet of the Omnetics ZIF adaptor and the Intan RHD132 board, both present in Appendix C.

3.1. Electrochemical Impedance (EI)

The analysis of the impedance modulus at 1 kHz is considered essential to determine how a specific ECoG device will perform. Measurements were repeated four times for each TrECoG. The final values

were calculated by averaging the data of the channels correspondent to each of the electrodes, the standard deviation was also determined at this time. The values obtained for each of the electrodes are shown in table 1. Also, the stability of the IZO SM devices was tested by measuring the impedance variation over a period of 40 days, where between the day 1 and the day 3 the device was used for recording brain activity the results are shown on table 2. After each test, the device was rinsed with distilled water and kept at room temperature.

Table 1 – Table containing all Impedance data acquired for the five devices fabricated.

	IZO SM (KΩ)	**GZO SM (KΩ)**	**IZO PL0 (KΩ)**	**IZO PL1 (KΩ)**	**IZO PL2 (KΩ)**
ELECTRODE 1	GND/Reference Short-Circuited	GND/Reference Short-Circuited	56.0 ± 1.0	48.9 ± 0.7	111.0 ± 0.8
ELECTRODE 2	42.4 ± 0.5	33.4 ± 1.3	59.6 ± 1.0	54.9 ± 0.5	71.7 ± 1.0
ELECTRODE 3	43.5 ± 3.7	29.3 ± 0.9	58.2 ± 1.3	47.5 ± 0.5	90 ± 6.2
ELECTRODE 4	45.8 ± 0.7	46.5 ± 0.9	57.0 ± 1.3	50.0 ± 0.6	1640.0 ± 10.6

The data shown in table 1 indicates that all devices, except the IZO Pl2, have interfacial impedances contained in the optimum range previously determined (1 – 100 kΩ). The lowest impedance was obtained for the GZO SM devices, 29.3 kΩ. In general, these values are considerably lower than the graphene ECoGs previously presented (243.5 kΩ). Regarding electrode material, the impedance differences previously demonstrated for the GZO and IZO devices could be explained by the morphology of their surface. GZO thin films could have a higher active area available due to their crystalline phase and grain boundaries, thus forming a more irregular surface, whereas IZO films are amorphous, leading to smoother surfaces with less active area. Further studies to analyze the surface morphology and crystallinity for both materials are required, such as SEM and DRX. Moreover, more devices should be fabricated and the impedance of the electrodes measured. Nevertheless, we showed that these two materials could be used as new electrode material.

No major differences in impedance were found between the SM and Pl devices, nevertheless, Pl TrECoGs have a higher impedance than SM. The major difference was found for the IZO Pl2 device. Impedance values for this TrECoG reached the upper limit previously established for the impedance, or even surpass it completely, this could be the result of impurities left from the photoresist, which could have been implanted on the thin film during the second plasma treatment. The effect of plasma treatments in the

thin film adhesion did not have a visible effect, for this reason, future works do not require this step, as it increases the devices' impedance with no better output than the standard fabrication steps.

The GZO SM and the IZO SM devices present the lowest impedances, these will be the devices considered for *in vivo* recordings.

Table 2 – Impedance variation for the IZO SM device. Day 1 measurements were taken one day before surgery (Day 2). Data taken over a 40 days period shows that there is significant variation in impedance.

	Day 1 (kΩ)	**Day 3 (kΩ)**	**Day 10 (kΩ)**	**Day 20 (kΩ)**	**Day 40 (kΩ)**
Electrode 1	-	-	-	-	-
Electrode 2	52.4 ± 1.1	99.4 ± 0.8	88.2 ± 1.3	78.6 ± 0.8	537.2 ± 2.7
Electrode 3	47.2 ± 2.0	89.8 ± 3.4	84.8 ± 1.4	73.6 ± 0.8	47.8 ± 0.4
Electrode 4	47.4 ±0.9	48.8 ± 1.0	44.4 ± 0.5	43 ± 0	38.8 ± 0.4

As it is possible to observe in table 2, there was a significant increase in impedance after the surgery, this could be caused by the presence of residues from the biological tissue, which covered the electrode area. After each test it is possible to observe a decrease in impedance, and even a full recuperation after the 40 days period. This observation leads to the fact that the increase in impedance was due to impurities left on the TCOs' surface, impurities which degraded over time during the 40 days period allowing them to be washed with ease. Nevertheless, the 2nd electrode was degraded along time. More statistical analysis need to be performed to evaluate the reliability of those devices along time.

3.2. Spectrophotometry

Spectrophotometry allows for the acquisition of data regarding the transmittance of a thin film. For this application the region of interest is contained in the visible range of the light spectrum (390 – 700 nm), especially for the green portion (532 nm), as green lasers are widely used in techniques previously described. In figure 11, it can be seen that GZO has a higher transmittance for a portion of the visible light (580 – 700 nm), nevertheless, IZO has a higher transmittance for the green band (89% IZO vs 85% GZO). These values exclude the substrate, the corning glass, and do not correspond directly the transmittance of

the actual devices, despite this fact, the values ranged between 70% and 90% for the produced TCO thin films which could be validated as efficient for the final application.

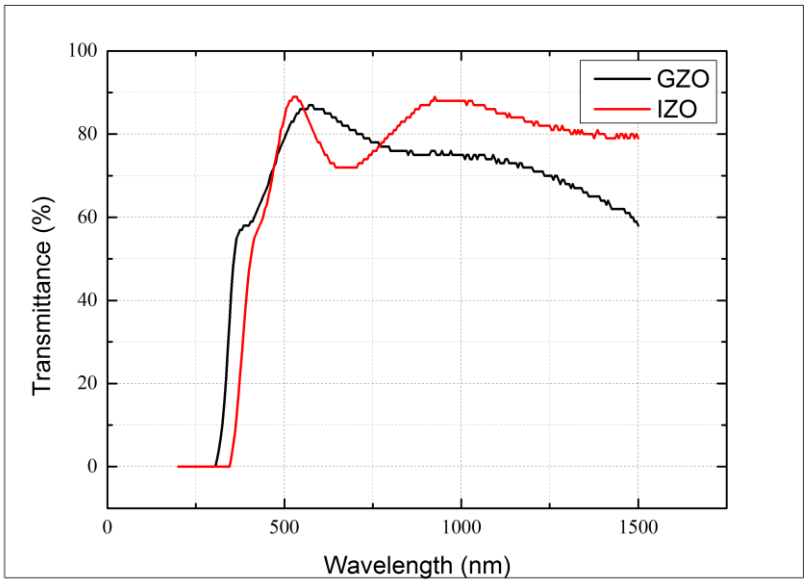

Figure 11 – Spectrophotometry of the IZO and GZO layers on a corning glass substrate.

3.3. Profilometry

Table 3 – Thickness values of the three main layers of the TrECoG devices.

	LAYER THICKNESS (NM)	
METAL LAYER (AU-TI)	99.8 ± 3.9	
ELECTRODE MATERIAL (TCO)	141.6 ± 60.1 (**GZO**)	253.4 ± 10.5 **(IZO)**
PARYLENE PASSIVATION LAYER	1499.8 ± 118.6	

The film thicknesses (table 3) measured through profilometry allowed for the establishment of standard values for future development of these devices. Since the goal of this work was to fabricate efficient transparent ECOG devices, no more studies were conducted regarding film thickness impact in the devices' behavior. Nevertheless, the standard deviation for the GZO deposition is much higher than expected,

indicating some type of error on the layer thickness measurements, further studies to assess the origin of this error are required.

3.4. *In Vivo* testing

3.4.1. Whisker stimulation and Barrel Cortex measurements

The tests conducted in this chapter represent the data acquired that validates these devices for *in Vivo* recordings. As explained earlier, these tests were conducted on anesthetized rodents (figure 12). The activation of the barrel cortex has been linked to inputs originated from the whiskers, and it is widely accepted that this area contains information regarding whisker functionality. [32].

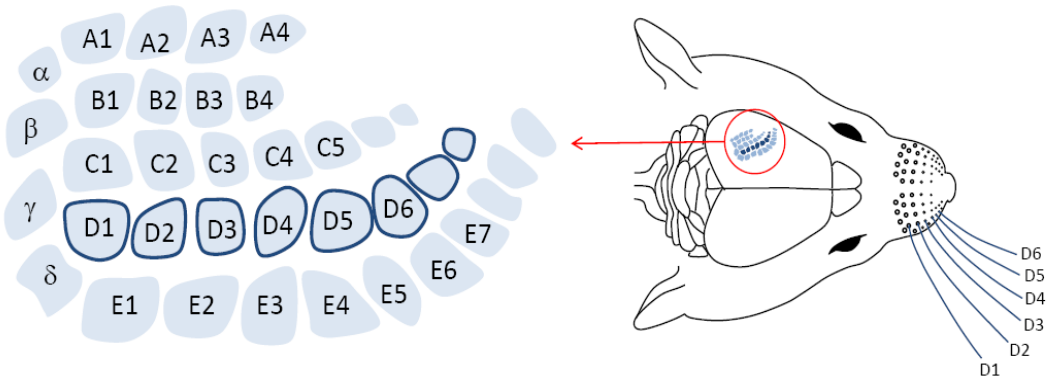

Figure 12 – Map of the barrel cortex of the rat's brain. Adapted from [33]

The TrECoGs were placed over the DE area, which links to some of the larger whiskers. According to recent studies [34], the stimulation of the whiskers generates a response in the barrel cortex with a 10 ms latency. A study regarding large neural networks also demonstrated that although whiskers are controlled contra-laterally, there's also an evoked response in the ipsi-lateral area, although of smaller amplitude [35].

In figure 13, the responses obtained by using the GZO SM device are shown. The blue line is the piezoelectric signal, averaged from all the hits. As one can see in figure 13.a, for the contra-lateral experiments, there is a considerable increase in electrical activity, with a signal increase of 400 µV for all electrodes, after an elapsed period of 15 ms. An approximate variation, of 300 µV, can also be seen for the ipsi-lateral measurements, nevertheless, for this case, the signal seems to attenuate sooner, facts that are in accordance with the information from previous studies. All the trials are plotted in figures 14.a and 14.b to demonstrate the dispersion of the data acquired with the GZO SM device. There is an artifact in the signal which arises prior to the stimulus applied, this is due to the fact that stimulations that occur inside the

refractory period defined during the data analysis have an effect which can be seen in the averaged data for the 4th electrode (blue line).

There was some noise originated from the piezoelectric sensor, nevertheless, it didn't seem to influence the signal, as it appeared at the time of the piezoelectric pulse, followed its wave form and vanished right after. For this reason, the pictures showed before are thought to be the best proof of the functionality of the devices produced. On the other hand, the effect of whisker stimulation in electrical activity of the barrel cortex is much more visible for the GZO SM device measurements.

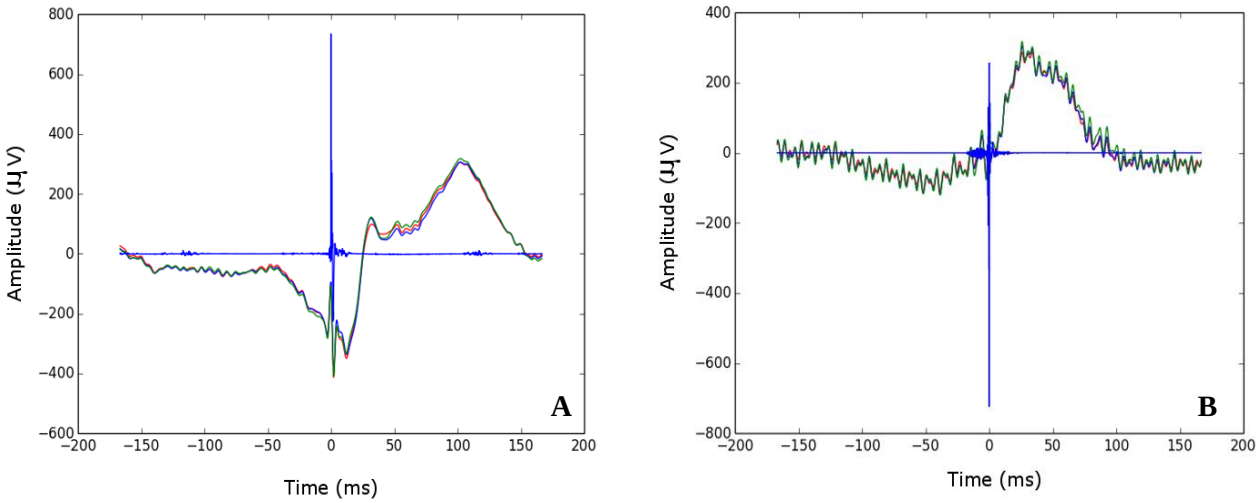

Figure 13 - Averaged signal acquired with the GZO SM device for the contra-lateral (A) and ipsi-lateral (B) barrel cortex.

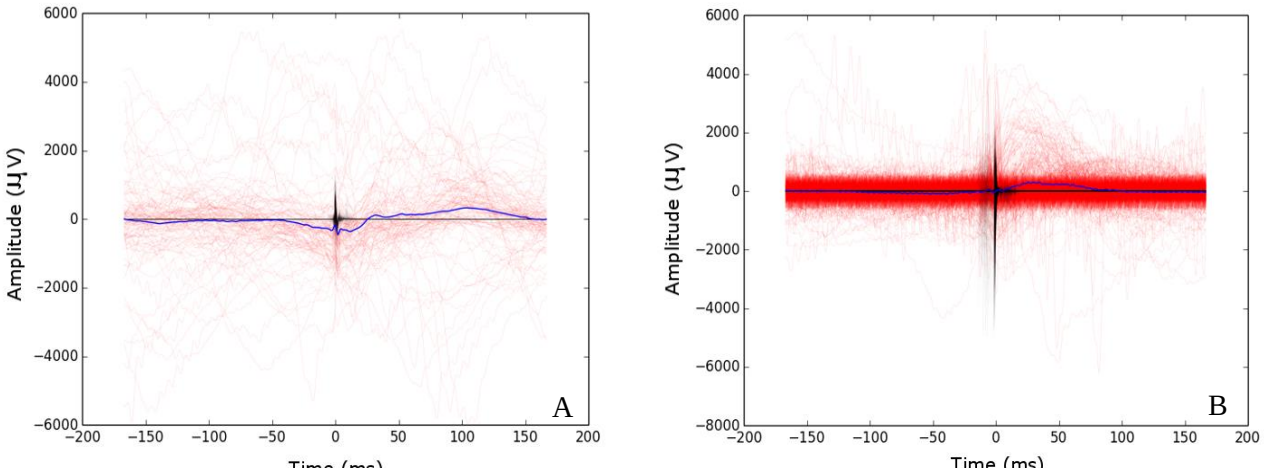

Figure 14 - All the trials acquired with the GZO SM device for the contra-lateral (A) and ipsi-lateral (B) barrel cortex.

3.5. Laser light pulse

In these experiments, graphical data demonstrates the impact produced by hitting the TrECoG electrodes with a green collimated light. In order to assess noise origin, three different types of tests were

conducted. 1) Laser directly aimed at the electrodes; 2) Laser aimed at the agar solution, 1 cm away from the electrodes; 3) Laser turned off, only the Arduino board is generating signal.

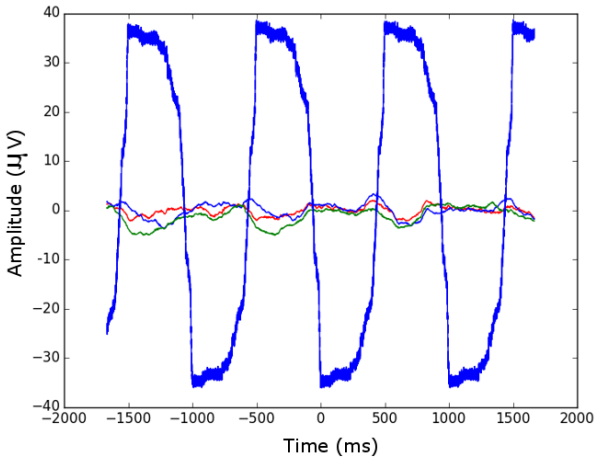

Figure 15 – Noise generated only by the Arduino board.

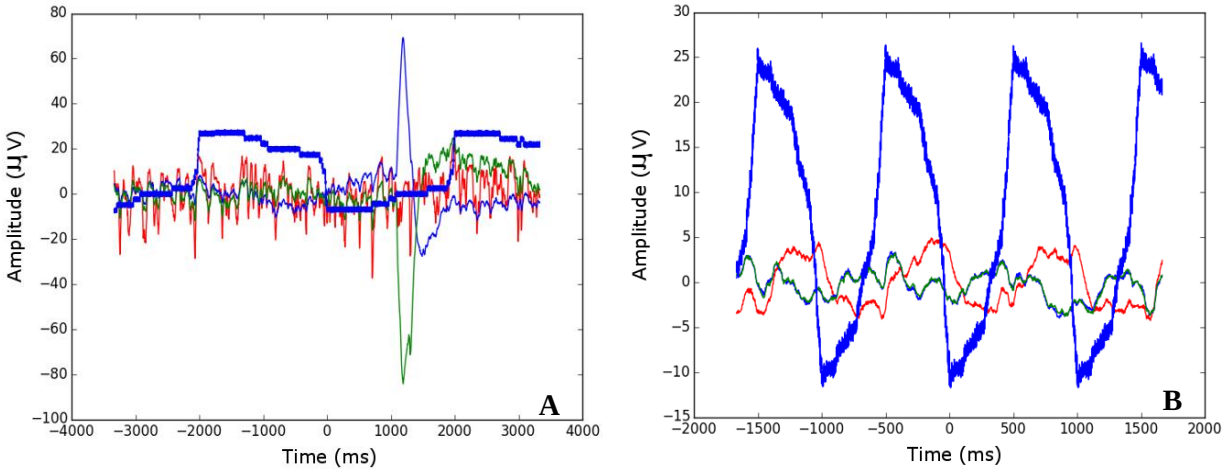

Figure 16 - Averaged laser noise with the light aimed 1 cm away from the electrodes of the GZO (A) and IZO (B) devices.

Starting with the noise generated from the Arduino board. As one can see in figure 15, The 1 s pulses generated by the Arduino board, the square wave, generate no observable variations in the signal recorded with the TrECoGs.

When recording with the laser light hitting the 1 cm away from the electrodes, there was no considerable signal noise, both for the GZO SM (figure 16.a) and the IZO Pl0 (figure 16.b).

There is noticeable noise, resulting from when the laser was hitting the electrodes directly. This type of noise was expected, as the TrECoGs transparency is not perfect. This noise could also arise from some of the light being scattered in the surface of the electrodes, or being reflected in the surface of the agar, finally hitting the gold lines, event that could cause the noise seen in figures 17.a and 17.b. But since we know the

frequency of the induced noise, it is possible to remove digitally by filtering the signal. Furthermore, considering that the peak to peak amplitude of the noise generated has a maximum value of 100 µV for the GZO SM device, one could still distinguish this noise from the signal acquired *in Vivo*, as can be seen previously, given the fact that the brain signal generates a response over 300 µV.

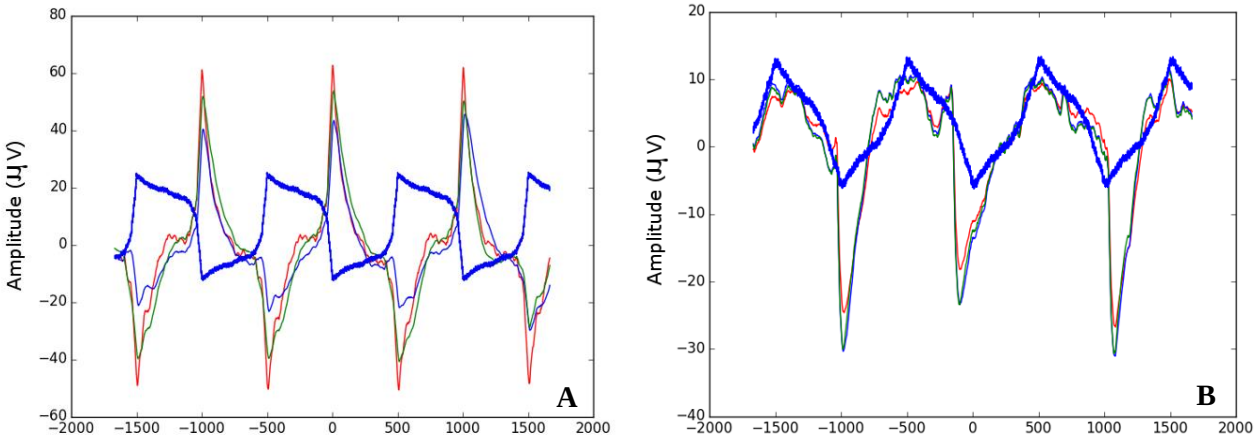

Figure 17 - Averaged laser noise with the light aimed directly at the electrodes of the GZO (A) and IZO (B) devices.

4. Conclusion and Future Perspectives

TrECoGs sensors enable new possibilities in the world of neuroscience. Taking light sensitive nanoparticles to the brain, modifying neurons to react to an exterior source of light or simply taking a picture of the brain while recording its electrical activity are all techniques that can benefit from the development of devices such as the ones produced in this work.

Previous works used ITO and Graphene sheet ECoGs, but no references were found regarding other TCOs, which could offer cheaper and simpler solutions. During this work, five types of TrECoGs sensors were produced. A Gallium Zinc Oxide device, patterned through shadow-masking. This device presented small response to the green light, good recording abilities and low impedances for all the electrodes. An Indium Zinc Oxide device, patterned through shadow-masking, which also demonstrated to be efficient in recording brain activity. After testing the materials with shadow masking, three IZO devices produced through photolithography and lift-off processes were tested. Despite the higher impedances found for the devices produced by this technique (IZO-SM 40 kΩ vs Pl IZO-60 kΩ) further studies should be performed using the Pl since it allows to increase the number of electrodes and to achieve the electrode's area found in the state of the art.

The TrECoG GZO SM, presented the best overall characteristics, a minimum of 29.3 kΩ impedance for electrodes with an electrode diameter of 500 µm, and an 84% transmittance for the green portion of the visible light. It was also capable of acquiring brain data efficiently, as demonstrated in the Results and Discussion. Simultaneously, it demonstrated a low noise when hit with a laser light.

For future work there is much to be done: The process of photolithography and lift off used for the production of these devices should be optimized, as it originated the devices with higher impedances, but it is also the technique with potential of producing smaller electrode sizes. No critical difference in film adhesion was observed by applying plasma treatments, nevertheless, film adhesion dramatically improved when the parylene C substrate switched from the ones used for the mechanical masks, to the thin films deposited on corning glass. For this reason, the next step would be to use the knowledge acquired in this work and fabricate a TrECoG with 4 channels and 20 µm lines that lead to 100 µm diameter transparent electrodes. Reduction of the electrode area would lead to higher impedances, and to inefficient devices. To this problem, coatings such as PEDOT:PSS nanotubes or silver nanowires could be a good start in order to diminish the increase in impedance. Overall, this work validated IZO and GZO as efficient devices for the fabrication of Transparent Electrocorticography sensors, and opened the path to a denser and smaller grid fabricated with materials that are of common use nowadays.

5. References

[1] Neuroscience Exploring the Brain, 3rd edition, Mark F. Bear, Barry W. Connors, Michael A. Paradiso, Lippincot Williams & Wilkins, 2007

[2] Neural Stimulation and Recording Electrodes, Stuart F. Cogan, Annu. Rev. Biomed. Eng. 2008. 10.275-309, 2008

[3] An Implantable 455-Active-Electrode 52-Channel CMOS Neural Probe, C. M. Lopez et al., ISSCC 2013/ Session 16/ Biomedical Circuits & Systems/ 16.2

[4] Multilayered Polypyrrole-Coated Carbon Nanotubes To Improve Functional Stability and Electrical Properties of Neural Electrodes, H. Chen, et al., ACS Publications,The Journal of Physical Chemistry, 2011

[5] Long-term culture of pluripotent stem-cell-derived human neurons on diamond – A substrate for neurodegeneration research and therapy, P. A. Nistor et al., Biomaterials 61 (2015) 139-149

[6] Niedermeyer's Electroencephalography: Basic Principles, Clinical Applications and Related Fields, Sixth Edtion, Donald L. Schomer, Fernando H. Lopes da Silva, Lippincot Williams & Wilkins, 2001

[7] Hand movement direction decoded from MEG and EEG, S. Waldert et. Al., The Journal of Neuroscience, 23 January 2008, 28(4): 1000-1008; doi: 10.1523/JNEUROSCI.5171-07.2008

[8] Principles of Neural Science, 5th edition, Eric R. Kandel, Mc.Graw-Hill Medical 2013

[9] Current source-density method and application in cat cerebral cortex: investigation of evoked potentials and EEG phenomena, Mitzdorf U. Physiol Rev 1985;65:37–100.

[10] The Brainweb: Phase Synchronization and Large-Scale Integration, Varela F., Nature Reviews Neuroscience Vol.2, April 2001, MacMillan Magazines Ltd.

[11] Coherent oscillatory activity in monkey area v4 predicts successful allocation of attention, Taylor, K., Mandon, S., Freiwald, W.A., Kreiter, A.K., 2005. Cereb. Cortex 15,1424–1437.

[12] More than spikes: common oscillatory mechanisms for content specific neural representations during perception and memory, Andrew J. Watrous, Current Opinion in Neurobiology 2015, 31:33–39

[13]http://www.lifesciences.ieee.org/publications/newsletter/april-2012/96-building-brain-machine-interfaces-neuroprosthetic-control-with-electrocorticographic-signals, as seen in 2/09/2015

[14] LFP and oscillations—what do they tell us?, Karl J Friston, Current Opinion in Neurobiology 2015, 31:1–6

[15] How Local Is the Local Field Potential? Yoshinao Kajikawa1, and Charles E. Schroeder1,2 - Neuron 72, 847–858, December 8, 2011 ª2011 Elsevier Inc

[16] Fabrication of Responsive, Softening Neural Interfaces, Taylor Ware Adv. Funct. Mater. 2012, 22, 3470–3479

[17] The effect of micro-ECoG substrate footprint on the meningeal tissue response. Schendel AA, Nonte MW, Vokoun C, Richner TJ, Brodnick SK, Atry F, et al., Neural Eng 2014;11:046011.

[18] Dissolvable films of silk fibroin for ultrathin conformal bio-integrated electronics. Kim DH, Viventi J, Amsden JJ, Xiao J, Vigeland L, Kim YS, et al. Nat Mater 2010;9:511–7.

[19] In vivo recordings of brain activity using organic transistors, Dion Khodagholy, NatureCommunications, 2013 4:1575

[20] High Resolution Electroencephalography in Freely Moving Mice, Jee Hyun Choi, J Neurophysiol 104: 1825–1834, 2010. First published July 7, 2010

[21] A Multi-Channel, Flex-Rigid ECoG Microelectrode Array for Visual Cortical Interfacing, Elena Tolstosheeva, Sensors 2015, 15, 832-854

[22] Cortical stimulation mapping using epidurally implanted thin-film microelectrode arrays, Katiuska Molina-Luna, Journal of Neuroscience Methods 161 (2007) 118–125

[23] Fabrication And Testing of a Large Area, High Density, Parylene MEMS µ-ECoG Array, P. Ledochowitsch1, P. Ledochowitsch, R. J. Felus, R. R. Gibboni, A. Miyakawa, S. Bao, and M. M. Maharbiz, "Fabrication and testing of a large area, high density, parylene MEMS," in 2011 IEEE 24th International Conference on Micro Electro Mechanical Systems, 2011, pp. 1031–1034.

[24] NeuroGrid: recording action potentials from the surface of the brain, Dion Khodagholy1, nature NEUROSCIENCE advance online publication, published online 22 December 2014

[25] An Optically Transparent, Gold-ITO-Hybrid Electrode Array for Integration of Electrocorticography with Optogenetic Techniques, Peter Ledochowitsch, P. Ledochowitsch, E. Olivero, T. Blanche, and M. M. Maharbiz, EEE Engineering in Medicine and Biology Society. Conference, vol. 2011, pp. 2937–40, Jan. 2011.

[26] Graphene-based carbon-layered electrode array technology for neural imaging and optogenetic applications, Dong-Wook Park, Nature Communications 5,Article number:5258

[27] Basic materials physics of transparent conducting oxides, P. P. Edwards, Dalton Trans., 2004, 2995-3002

[28] New And Sustainable Photovoltaics – The Physics of Transparent Conducting Oxides[1], R. Treharne, 2014

[29] Highly stable transparent and conducting gallium-doped zinc oxide thin films for photovoltaic applications, E. Fortunato et al., Solar Energy Materials & Solar Cells 92 (2008) 1605–1610

[30] Properties of Indium-Zinc-Oxide Thin Films Prepared by Facing Targets Sputtering at Room Temperature, You Seung Rim , Journal of the Korean Physical Society, Vol. 54, No. 3, March 2009, pp. 1267_1272

[31] Bonsai: An event-based framework for processing and controlling data streams, Lopes G, Bonacchi N, Frazão J, Neto JP, Atallah BV, Soares S, Moreira L, Matias S, Itskov PM, Correia PA, Medina RE, Calcaterra L, Dreosti E, Paton JJ, Kampff AR.Frontiers in Neuroinformatics. 2015; 9:7.

[32] Sensory and cognitive neurophysiology in rats, Part 1: Controlled tactile stimulation and micro-ECoG recordings in freely moving animals, Dimitriadis G., Journal of Neuroscience Methods 232 (2014) 63–73

[33] http://www2.psy.unsw.edu.au/users/earabzadeh/Research.html, as seen in 23 Set 2015

[34] Sensory and cognitive neurophysiology in rats. Part 2: Validation and demonstration, Dimitriadis G., J Neurosci Methods. 2014 Jul 30;232:47-57

[35] A mouse model for studying large-scale neuronal networks using EEG mapping techniques, Mégevand P., Volume 42, Issue 2, 15 August 2008, Pages 591–602

6. Appendix

6.1. Appendix A – Mechanical Mask and Photolithography Pattern

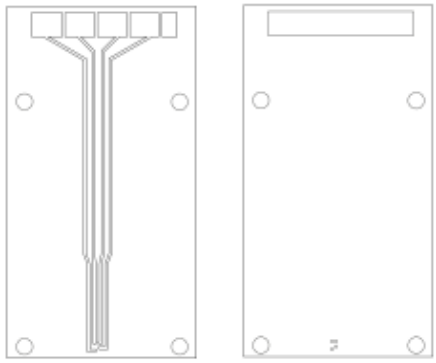

Figure 17 – Mechanical aluminum masks to pattern the lines (left) and to open the contacts and electrodes (right).

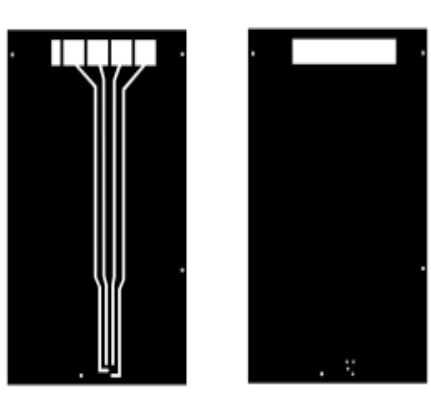

Figure 16 – Optical acetate sheet masks to pattern the lines (left) and to open the contacts and electrodes (right).

6.2. Appendix B – Deposition conditions for IZO and GZO and Plasma etching.

Table 4 - Deposition conditions for IZO and GZO and Plasma etching.

SYSTEM	3 Target Sputtering System
MATERIAL	IZO
P (O_2)	1 x 10^{-5} mbar
P (Ar)	7 x 10^{-3} mbar
$P_{DEPOSITION}$	7 x 10^{-3} mbar
POWER	50 W
DEPOSITION TIME	80 min
SYSTEM	AJA ATC 1300 Sputtering
MATERIAL	GZO
H_2 FLOW	0.5 sccm
Ar FLOW	50 sccm
$P_{DEPOSITION}$	2.26 x 10^{-3} mbar
POWER	150 W
DEPOSITION TIME	30 min
SYSTEM	RIE Trion (Plasma Etching)

O_2 FLOW	10 sccm
PRESSURE	6.67 x 10^{-2} mbar
POWER	50 W
ETCHING RATIO FOR PARYLENE C	1.6 nm/s

6.3. Appendix C – ZIF sheet and RHD 132 schematic

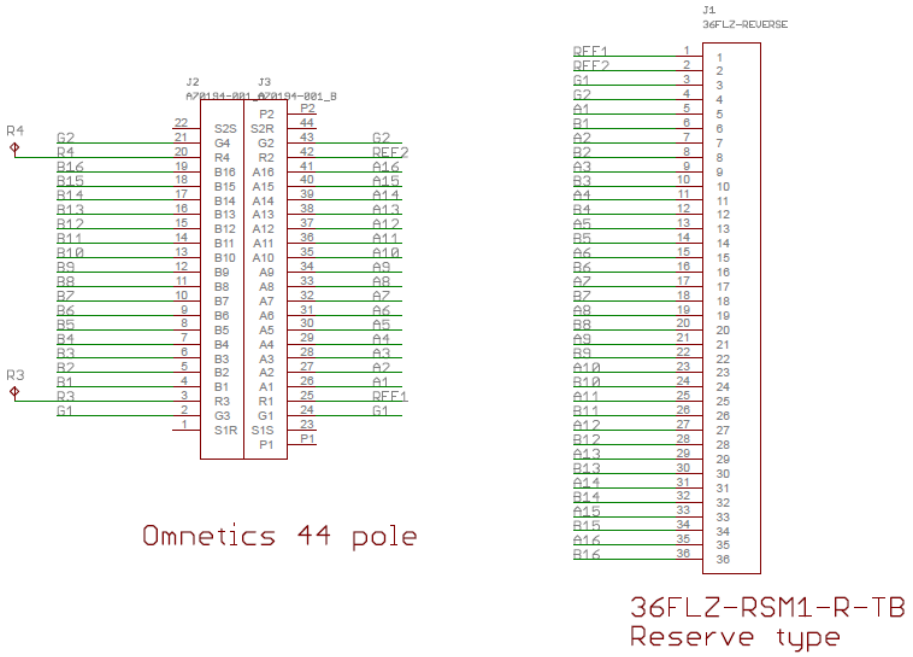

Figure 18 – ZIF channels, the Intan board connects from R3 to R4 and from R1 to R1.

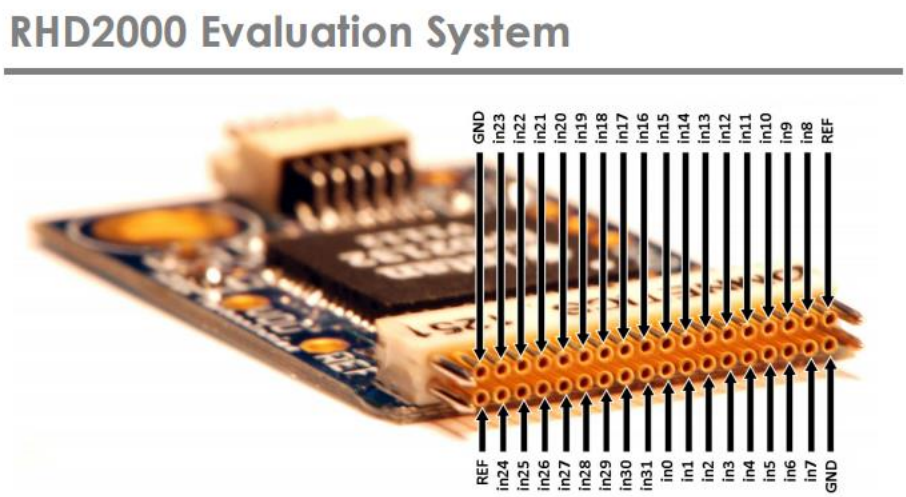

Figure 19 – Intan board.

6.4. Appendix D – Python code

```
import os
import numpy as np
import scipy.signal as signal

def loadRawData(filename,numChannels,dtype):
    fdata = np.fromfile(filename,dtype=dtype)
    numsamples = len(fdata) / numChannels
    data = np.reshape(fdata,(numsamples,numChannels))
    return (np.transpose(data))

def loadAdcAmplifierData(filename):
    adc = loadRawData(filename,numChannels=8,dtype=np.uint16)
    pathsplit = os.path.split(filename)
    filename = os.path.join(pathsplit[0],pathsplit[1].replace('ADC','AMP'))
    amplifier = loadRawData(filename,numChannels=32,dtype=np.uint16)
    amplifier= ((np.float32(amplifier) - 32768) * 0.195).astype(np.int32)
    return adc, amplifier

def find_peaks(data,threshold,minstep=0):
    derivative = np.diff(np.sign(np.diff(data)))
    if threshold > 0:
        derivative = derivative < 0
    else:
        derivative = derivative > 0
```

```
    peaks = derivative.nonzero()[0] + 1 # local max
    if threshold > 0:
        peaks = peaks[data[peaks] > threshold]
    else:
        peaks = peaks[data[peaks] < threshold]

    if minstep > 0:
        gpeaks = split_list_pairwise(peaks,lambda x,p:x-p > minstep)
        peaks = np.array([g[np.argmax([data[i] for i in g])] for g in gpeaks])
    return peaks

def split_list_pairwise(l,p):
    groups = []
    prev = None
    group = None
    for x in l:
        if prev is None or p(x,prev):
            group = []
            groups.append(group)
        group.append(x)
        prev = x
    return groups

def align_data(data,indices,before=0,after=0):
    columns = np.shape(data)[1]
```

```
    return [data[:,slice(index-before,index+after+1)] for index in indices if index-before >= 0 and index+after < columns]


def find_edges(data, threshold, inter_spike_distance=300):


    samples= np.arange(0,np.shape(data)[0])#trigchannel

    spike_times = np.array([x for x in samples if (data[x] < threshold)])

    diff_spikes_times = np.diff(spike_times)

    spike_times = np.array([x for i, x in enumerate(spike_times[:-2]) if (diff_spikes_times[i] > inter_spike_distance)])

    return spike_times


def highpass(data,BUTTER_ORDER=3, F_HIGH=7500,sampleFreq=20000.0,passFreq=150.0):

    b, a = signal.butter(BUTTER_ORDER,(passFreq/(sampleFreq/2), F_HIGH/(sampleFreq/2)),'pass')

    #return signal.lfilter(b,a,data)

    return signal.filtfilt(b,a,data)


def lowpass(data,BUTTER_ORDER=3, F_HIGH=150,sampleFreq=20000.0):

    b, a = signal.butter(BUTTER_ORDER, F_HIGH/(sampleFreq/2),'lowpass')

    #return signal.lfilter(b,a,data)

    return signal.filtfilt(b,a,data)


def notch(data,BUTTER_ORDER=3,flow=40,F_HIGH=60,sampleFreq=20000.0):

    b, a = signal.butter(BUTTER_ORDER,(  flow/(sampleFreq/2), F_HIGH/(sampleFreq/2)),'bandstop')

    #return signal.lfilter(b,a,data)

    return signal.filtfilt(b,a,data)
```

```
def normalize(data):
    return data - np.reshape(np.mean(data,1),[8,1])
def juxta_trigger_analysis(filename,triggerchannel=5,threshold=-
2,minstep=2500,before=15000,after=15000,gain=1.0):
    global adc, amplifier, adc_scaled_mV, filtamplifier,trigchannel, triggers, alignadc, alignamplifier,
alignamplifier_raw

    adc, amplifier = loadAdcAmplifierData(filename)
    factor_scale= 10.0/(65536*gain)
    adc_scaled_mV_offset= normalize(adc[:,:])
    adc_scaled_mV =(adc_scaled_mV_offset[:,:])*factor_scale
    trigchannel = adc_scaled_mV[triggerchannel,:]
    triggers = find_peaks(trigchannel,threshold,minstep) # Trigger on spikes
    filtamplifier = highpass(amplifier[:,:])
    alignadc = np.dstack(align_data(adc_scaled_mV[:,:],triggers,before,after))
    alignamplifier = np.dstack(align_data(filtamplifier[:,:],triggers,before,after))
    alignamplifier_raw = np.dstack(align_data(amplifier[:,:],triggers,before,after))

#plot

def triggerline(x,**kwargs):
    if x is not None:
        ylim = plt.ylim()
        plt.vlines(x,ylim[0],ylim[1],**kwargs)
```

```
def plot_triggers_single_channel(triggerdata,channel,trigger=None,**kwargs):
    number_samples=np.shape(triggerdata)[1]
    time_msec=number_samples/30.0
    x_adc=np.linspace(-(time_msec/2), (time_msec/2), num=number_samples)
    for t in range(np.shape(triggerdata)[2]):
        data = triggerdata[channel,:,t]
        plt.plot( x_adc,data,**kwargs)  #####  mV andf msec
    triggerline(trigger)

def plot_triggers_single_channel_average(triggerdata,channel,trigger=None,**kwargs):
    global data
    data = np.mean(triggerdata[channel,:,:], axis = 1)
    number_samples=np.shape(triggerdata)[1]
    time_msec=number_samples/30.0
    x_adc=np.linspace(-(time_msec/2), (time_msec/2), num=number_samples)
    plt.plot(x_adc,data,**kwargs)
    triggerline(trigger)

def plot_trigger_average_mapp(triggerdata,channeloffset=0,trigger=None,**kwargs):
    global data, x_adc

    data = np.mean(triggerdata,axis=2)
    #data=triggerdata
    number_samples=np.shape(triggerdata)[1]
    time_msec=number_samples/30.0
    time_samples= number_samples
```

```
    x_adc=np.linspace(-(time_msec/2), (time_msec/2), num=number_samples)
    #x_adc=np.linspace(0, time_samples, num=number_samples)
    #x_adc=np.linspace(0, time_msec, num=number_samples)
    #rect_data= data - np.reshape((np.mean(data[:,[0, (number_samples/2)-500]],1)),[32,1])
    #baseline = np.mean(data[:, [beginSample, endSample]], 1)
    plt.plot(x_adc, data[29,:].T + channeloffset*2, 'r', **kwargs)
    plt.plot(x_adc, data[2,:].T + channeloffset*3, 'b', **kwargs)
    plt.plot(x_adc, data[15,:].T + channeloffset*8, 'g', **kwargs)
    triggerline(trigger)

def plot_trigger_average_mapp2(triggerdata,channeloffset=0,trigger=None,**kwargs):
    global data, x_adc

    data = np.mean(triggerdata,axis=2)
    #data=triggerdata
    number_samples=np.shape(triggerdata)[1]
    time_msec=number_samples/30.0
    time_samples= number_samples
    x_adc=np.linspace(-(time_msec/2), (time_msec/2), num=number_samples)
    for i in np.arange(32):
        plot(x_adc, data[i,:].T +channeloffset*i)
```

Order for code use:

```
adc, amplifier = loadAdcAmplifierData()
factor_scale= 10.0/(65536*gain)
adc_scaled_mV_offset= normalize(adc[:,:])
adc_scaled_mV =(adc_scaled_mV_offset[:,:])*factor_scale
trigchannel = adc_scaled_mV[triggerchannel,:]
figure(); plot(trigchannel)
threshold = 0.1
minstep = 2500
before = 5000
after = 5000
triggers = find_peaks(trigchannel,threshold,minstep)
notchlowamplifier=notch(amplifier)
lowamplifier= lowpass(notchlowamplifier)
alignamplifier = np.dstack(align_data(lowamplifier[:,:],triggers,before,after))
alignadc = np.dstack(align_data(adc_scaled_mV[:,:],triggers,before,after))

figure(); plot_trigger_average_mapp(alignamplifier, channeloffset=100)
plot_triggers_single_channel_average(alignadc*1000,5)
```